Steady-State Analysis of the LLC Series Resonant Converter

James F. Lazar
Braxton Engineering, Inc.
28 Vista Mar Drive
Laguna Niguel, CA 92677
E-mail: jimlazar@ftel.net
(949) 249-2197

Robert Martinelli
Artesyn Technologies
5252 Bolsa Avenue
Huntington Beach, CA 92649-1019
E-mail: rob.martinelli@artesyn.com
(714) 899-6800 ext. 201

***Abstract*- The operating modes of the LLC series resonant converter are analyzed to determine the steady-state operating point and mode boundaries. The three-element LLC series resonant converter is realized by adding an inductor to the basic two-element series resonant converter topology. Unlike the two-element series resonant converter, which is limited strictly to step-down operation, the LLC converter is capable of both step-up and step-down. A wide range of output power is controlled with only a narrow variation in operating frequency. In addition, zero-voltage switching can be achieved over the entire operating range. All of these desirable properties are obtained essentially for free, as the additional resonant inductor can be realized simply by introducing an air gap to the main power transformer.**

I. INTRODUCTION

While the advantages of resonant power converters include high efficiency and low noise, the series resonant converter suffers from several drawbacks that limit its usefulness in many applications. First, the converter is theoretically incapable of regulating when unloaded. Second, a wide variation of frequency is necessary to provide regulation over even a moderate load range. Third, at light loads, the resonant current is reduced to a point where zero-voltage switching (ZVS) is lost.

To contend with these drawbacks, parallel, series-parallel, and many other higher-order resonant topologies [3,4] were developed. However, the LLC series resonant converter (LLC-SRC) (fig. 1) has been largely overlooked, owing perhaps to counterintuitive notion that the addition of magnetizing current in the primary resonant circuit can be of substantial benefit. In [1], above resonance operation of the LLC-SRC in buck mode is studied in detail. The author of [4] recognized the boost property of this topology, and also the narrow frequency range necessary for regulation. That paper, however, discusses a multitude of topologies, and therefore does not provide analytical detail. Reference [5] suggests that optimum performance is obtained by operating the topology at resonance, and switching at zero current. This, however, precludes ZVS. Above resonance operation is explored in [6] using the fundamental mode analysis approach. Below resonance waveforms are shown in [7], but no analysis is given. Reference [8] provides equations of state, but doesn't solve them. Rather, the low-noise aspects of this topology are explored. Finally, [9] provides a detailed analysis of above resonance operation, but is complicated by the inclusion of the transformer leakage inductance.

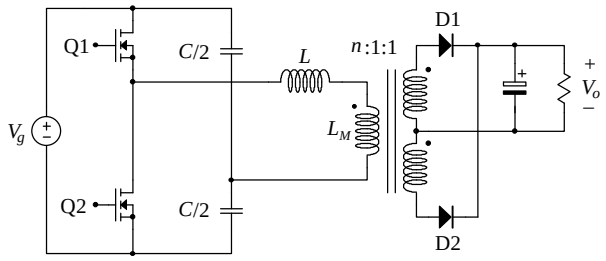

Figure 1: Half-Bridge realization of the LLC series resonant converter.

In this paper, a detailed analysis is given covering a broad operating range. It is found that the buck and boost modes possess different sets of steady-state operating modes, and these cases are looked at separately. Above and below resonance operation is discussed for each case. Normalized power curves are calculated, and these provide for a simple design procedure. The result is a low cost, high efficiency topology. Experimental results verify these claims.

II. ANALYSIS

Operation of the LLC-SRC is much like that of the basic two-element SRC. Switches are controlled in complementary fashion, at 50% duty, and variable frequency control is used to regulate the output voltage and current. A small dead-time is introduced to allow resonant switching transitions, and thus ZVS. In the analysis, these resonant transitions are ignored, and it is assumed therefore that a square-wave input drives the resonant network/rectifier. We consider frequencies from about half of the series tank resonant frequency, to infinity. All components are assumed to be ideal.

The LLC-SRC topology can be implemented as a half-bridge or full-bridge type, and the analysis presented here will cover either case by setting

$$\begin{aligned} V_1 &= V_g/2 \quad \text{(half-bridge)} \\ V_1 &= V_g \quad\quad \text{(full-bridge)} \end{aligned} \tag{1}$$

where V_1 is the amplitude of the input square-wave. In addition, the output rectifier may be implemented as a full-wave center-tapped configuration with *n*:1:1 turns ratio as shown in fig. 1, or as a full-wave bridge configuration with *n*:1 turns ratio, useful in high voltage applications. In either case, we have

$$V_2 = nV_O \tag{2}$$

where V_2 now represents the adjusted output voltage as seen by the resonant network.

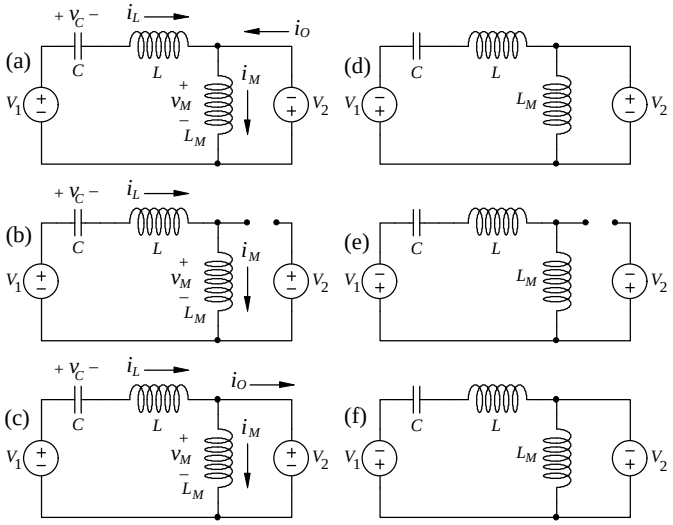

EQ. CKT.	(a)	(b)	(c)	(d)	(e)	(f)
Q1	ON	ON	ON	OFF	OFF	OFF
Q2	OFF	OFF	OFF	ON	ON	ON
D1	OFF	OFF	ON	ON	OFF	OFF
D2	ON	OFF	OFF	OFF	OFF	ON

Figure 2: A total of six equivalent circuits model the ideal LLC-SRC over a full cycle. Owing to symmetry, only three of these are necessary to completely characterize steady-state operation.

III. NORMALIZATION

The equations and results are normalized in order to generalize the results and simplify the design process. The normalized time variable θ is defined by

$$\theta \equiv \omega_0 t \tag{3}$$

where ω_0 is the resonant frequency of the series tank:

$$\omega_0 = 1/\sqrt{LC} = 2\pi f_0 \tag{4}$$

The steady-state is characterized by one complete period of converter operation, starting with a set of initial conditions at $\theta = 0$, and returning to these same conditions at the end of a full period. By symmetry however, the steady-state can instead be characterized by events occurring over a half-period, by ending the half-period with the values of states opposite those of the initial conditions. Hence, we need only consider a half-period of operation to determine steady-state, thereby simplifying the analysis. A normalized half-period is of length

$$\gamma \equiv \omega_0 \frac{T_S}{2} = \frac{\pi}{F} \tag{5}$$

where T_S is the switching period and F is the normalized switching frequency, given by

$$F \equiv \frac{f_S}{f_0} \tag{6}$$

Since the choice of the start of the half-period is arbitrary, we choose the half-period when transistor Q1 is on for simplicity. Hence, Q1 turns on at $\theta = 0$, and turns off at $\theta = \gamma$, at which time Q2 turns on. The voltage waveform incident to the converter is therefore a square-wave of amplitude V_1. For the purpose of steady-state analysis, the transition times are ignored.

The base quantities are chosen to simplify the design process. In the design of a typical dc-dc converter, the output voltage is regulated to a constant value, while the input voltage varies over some specified range. Therefore, it makes sense to choose the output rather than the input voltage as the basis for normalization, in order to keep the base quantities constant when evaluating varying operating conditions. With this in mind, we define the base quantities:

$$\begin{aligned} V_{\text{BASE}} &\equiv V_2 \\ \omega_{\text{BASE}} &\equiv \omega_0 = 1/\sqrt{LC} \\ R_{\text{BASE}} &\equiv R_0 = \sqrt{L/C} \\ I_{\text{BASE}} &\equiv V_2/R_0 \\ P_{\text{BASE}} &\equiv V_2^2/R_0 \end{aligned} \tag{7}$$

In forming normalized variables, lowercase *m* is used to denote normalized voltages and lowercase *j* to denote normalized currents. The subscripts of the original variables are retained. The normalized time variable is inserted by substituting $t = \theta/\omega_0$ into the time-domain expressions. Hence, in general, we have

$$\begin{aligned} m_X(\theta) &= \frac{v_X(\theta/\omega_0)}{V_{\text{BASE}}} \\ j_Y(\theta) &= \frac{i_Y(\theta/\omega_0)}{I_{\text{BASE}}} \end{aligned} \tag{8}$$

Although the base voltage is defined as V_2, the dc conversion ratio *M* is defined in the traditional manner

$$M \equiv \frac{V_2}{V_1} \tag{9}$$

When both output diodes are open, a second resonant frequency appears

$$\omega_1 \equiv 1/\sqrt{(L + L_M)C} \tag{10}$$

The ratio of the resonant inductance to the magnetizing inductance is defined

$$l \equiv L/L_M \tag{11}$$

and we define the ratio of the two resonant frequencies

$$k_1 \equiv \omega_1/\omega_0 = \sqrt{l/(1+l)} \tag{12}$$

In any half-period, $0 \le \theta \le \gamma$, there are a total of five intervals, some of which may or may not occur, in steady-state. The main power interval, denoted α_3, occurs in every half-period below cutoff. Cutoff is defined as the region of operation where zero power is delivered to the load, and occurs at frequencies above the cutoff frequency. In cutoff, there is a single α_2 interval that spans the entire half-period. Hence, in any half-period, in steady-state, it is required that

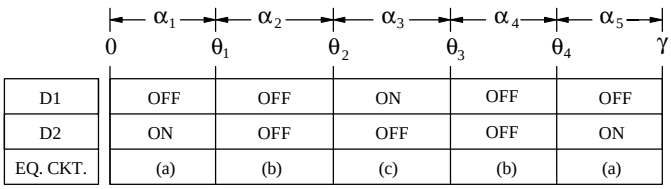

Figure 3: Timeline of a half-period (transistor Q1 on) showing the relation between normalized diode conduction intervals α_k and normalized switching times θ_k. Note that no steady-state operating mode actually contains all five intervals, as at least two of the α_k's are zero in every mode.

$$\sum_{k=1}^{5} \alpha_k = \gamma \tag{13}$$

As shown in figure 3, there are two intervals, each of which may or may not occur, preceding the main power interval α_3. During interval α_1, current flows to the output via diode D2, but is diminishing. Interval α_2 is an idling interval with both diodes D1 and D2 open.

Similarly, there are two intervals, each of which may or may not occur, following the main power interval α_3. Interval α_4 is an idling interval like α_2, and interval α_5 is similar to α_1, with current flow to the output via diode D2. Note that intervals α_2 and α_4 possess the same equivalent circuit, as do intervals α_1 and α_5.

IV. Buck Mode ($M < 1$)

When operating in buck, or voltage step-down mode, the converter passes through a series of five operating modes (fig. 4) as the frequency is swept from below resonance, through resonance, and to cutoff. Two of these modes are continuous conduction modes, two are discontinuous conduction modes, and cutoff itself is a mode. A continuous conduction mode (CCM) is defined as a mode in which the diodes conduct continuously throughout the cycle, and a discontinuous conduction mode (DCM) is defined as a mode in which both diodes are open over some finite interval.

A. Continuous Conduction Mode Above Resonance

The CCMA operating mode (fig. 5) exists over a range of frequencies from the resonant frequency to some frequency above resonance, for converters operating in buck ($M < 1$) mode. In this section, we develop a closed-form solution for this mode, paralleling a procedure presented in [2]. This mode is also described as the (α_1, α_3) mode, as these are the intervals that comprise the mode.

To begin, in the (α_1, α_3) mode, since $\alpha_2 = \alpha_4 = \alpha_5 = 0$, we have $\theta_2 = \theta_1$ and $\theta_3 = \gamma$ (see the timeline in fig. 4). Referring to the appendix, the normalized equations describing the resonant states are

$$\left.\begin{aligned} m_C(\theta) &= (m_C(0) - 1/M - 1)\cos\theta + \\ &\qquad j_L(0)\sin\theta + 1/M + 1 \\ j_L(\theta) &= (-m_C(0) + 1/M + 1)\sin\theta + j_L(0)\cos\theta \end{aligned}\right\} 0 \le \theta \le \theta_1 \tag{14a, 14b}$$

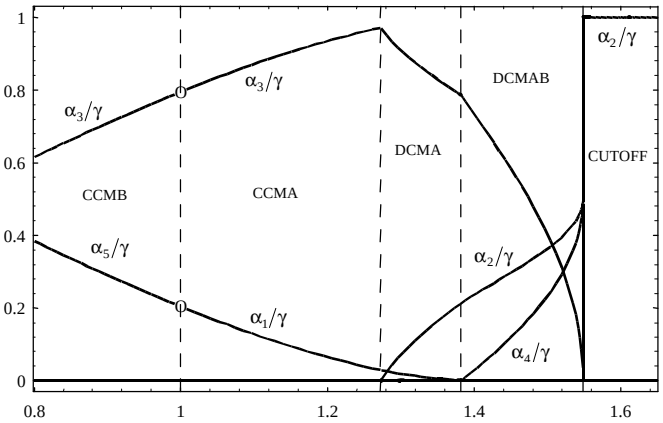

Figure 4: Plot of the normalized conduction intervals α_k/γ vs. normalized frequency F, in buck mode $(M = 0.8, l = 0.5)$. Note the discontinuity at $F = 1$, and the transition from CCMB to CCMA.

$$\left.\begin{aligned} m_C(\theta) &= (m_C(\theta_1) - 1/M + 1)\cos(\theta - \theta_1) + \\ &\qquad j_L(\theta_1)\sin(\theta - \theta_1) + 1/M - 1 \\ j_L(\theta) &= (1/M - 1 - m_C(\theta_1))\sin(\theta - \theta_1) + \\ &\qquad j_L(\theta_1)\cos(\theta - \theta_1) \end{aligned}\right\} \theta_1 \le \theta \le \gamma \tag{15a, 15b}$$

with unknowns $m_C(0)$, $j_L(0)$, $m_C(\theta_1)$, $j_L(\theta_1)$, and θ_1. From the waveforms in figure 5, we see that the voltage applied to the magnetizing inductance in CCM is a square-wave. The magnetizing current is therefore a triangle-wave, the valley of which occurs at $\theta = \theta_1$. At this instant, the resonant current and the magnetizing current are equal, the output current is zero, and the output diodes switch polarity. It is straightforward to show that the peak amplitude of the triangle wave is $\gamma l/2$, and that

$$j_M(\theta_1) = j_L(\theta_1) = -\gamma l/2 \tag{16}$$

Hence, the magnetizing current effectively "pins" the value of the resonant current at $\theta = \theta_1$. By symmetry, we have in steady-state

$$\begin{aligned} m_C(\gamma) &= -m_C(0) \\ j_L(\gamma) &= -j_L(0) \end{aligned} \tag{17}$$

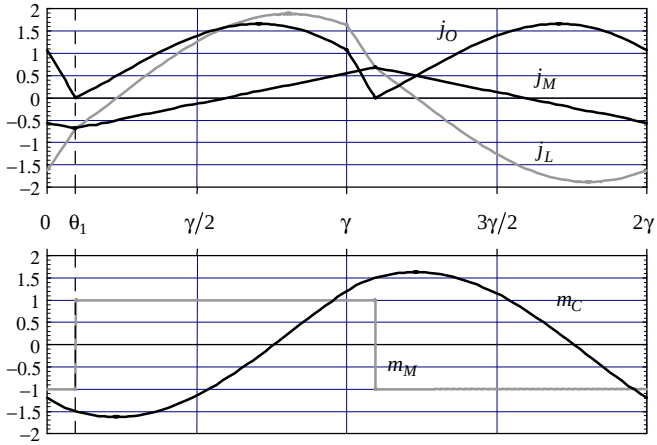

Figure 5: Buck mode CCMA, or (α_1, α_3) mode, normalized steady-state waveforms $(M = 0.8, l = 0.5, F = 1.15)$.

We now wish to solve for $m_C(0)$ and $j_L(0)$. The algebra is simplified by making the substitution

$$m_C(\theta) = m'_C(\theta) + 1/M + 1 \tag{18}$$

resulting in the primed system of equations

$$\left.\begin{aligned} m'_C(\theta) &= m'_C(0)\cos\theta + j_L(0)\sin\theta \\ j_L(\theta) &= -m'_C(0)\sin\theta + j_L(0)\cos\theta \end{aligned}\right\} 0 \le \theta \le \theta_1 \tag{19a, 19b}$$

$$\left.\begin{aligned} m'_C(\theta) &= (m'_C(\theta_1)+2)\cos(\theta-\theta_1) - \\ &\qquad (\gamma l/2)\sin(\theta-\theta_1) - 2 \\ j_L(\theta) &= (-m'_C(\theta_1)-2)\sin(\theta-\theta_1) - \\ &\qquad (\gamma l/2)\cos(\theta-\theta_1) \end{aligned}\right\} \theta_1 \le \theta \le \gamma \tag{20a, 20b}$$

with primed boundary conditions

$$\begin{aligned} m'_C(\gamma) &= -m'_C(0) - 2/M - 2 \\ j_L(\gamma) &= -j_L(0) \end{aligned} \tag{21}$$

Next, $m'_C(\theta_1)$ is eliminated from (20a) and (20b) by substituting $\theta = \theta_1$ into (19a). The primed boundary conditions (21) are then applied to arrive at expressions for $m'_C(0)$ and $j_L(0)$ as functions of θ_1 and $\gamma - \theta_1$. Next, evaluate (19b) at $\theta = \theta_1$, and apply the boundary condition (16). Now substitute into this result the expressions for $m'_C(0)$ and $j_L(0)$ just derived. Letting

$$\begin{aligned} \alpha_1 &= \theta_1 = \gamma/2 - \phi \\ \alpha_3 &= \gamma - \theta_1 = \gamma/2 + \phi \end{aligned} \tag{22}$$

and simplifying, we arrive at a closed form equation for $\sin\phi$ as a function of γ, l, and M:

$$\sin\phi = \frac{\gamma l M}{2}\cos\frac{\gamma}{2} + M\sin\frac{\gamma}{2} \tag{23}$$

Back substitution then yields

$$\begin{aligned} m_C(0) &= 1 - \cos\phi/\cos(\gamma/2) \\ m_C(\theta_1) &= \left(1 - \cos\phi/\cos(\gamma/2)\right)/M \\ j_L(0) &= \gamma l M/2 + \left(M - 1/M\right)\tan(\gamma/2) \\ j_M(0) &= -l\phi \end{aligned} \tag{24}$$

which completes the closed-form steady-state solution for the CCMA mode.

B. Continuous Conduction Mode Below Resonance

Analysis of the CCMB operating mode is basically the same as the CCMA mode. In buck mode, the CCMB mode exists from frequencies well below the resonant frequency up to resonance. At the resonant frequency, in buck mode, there is a discontinuity, where the resonant states and output power become infinite. Hence, driving the converter at resonance in buck mode is not allowed mathematically, as there is no finite steady-state solution. Note, however, that in practice this is not really a problem, for the following reasons: First, a real converter has resistance and other losses that inherently provide limiting. Second, it takes a finite number of cycles for the resonant states to build to a large value. Finally, a properly designed controller will act to prevent the over-current condition that results in this circumstance.

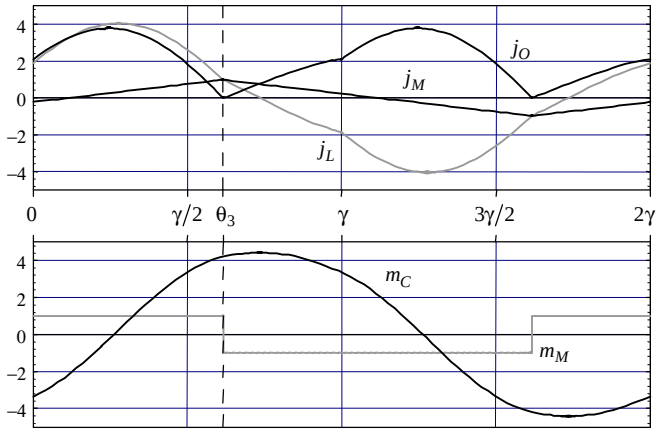

Figure 6: Buck mode CCMB, or (α_3, α_5) mode, normalized steady-state waveforms $(M = 0.8, l = 0.5, F = 0.8)$.

The CCMB, or (α_3, α_5) mode has a closed form solution

$$\begin{aligned} \alpha_3 &= \gamma/2 + \phi \\ \alpha_5 &= \gamma/2 - \phi \end{aligned} \tag{25}$$

with $\sin\phi$ given in (13). Also, we have

$$\begin{aligned} m_C(0) &= \left(\cos\phi/\cos(\gamma/2)\right) - 1 \\ m_C(\theta_3) &= \left(1 - \cos\phi/\cos(\gamma/2)\right)/M \\ j_L(0) &= \gamma l M/2 + \left(M - 1/M\right)\tan(\gamma/2) \\ j_L(\theta_3) &= j_M(\theta_3) = \gamma l/2 \\ j_M(0) &= -l\phi \end{aligned} \tag{26}$$

C. Discontinuous Conduction Mode Above Resonance

In buck mode, the DCMA or $(\alpha_1, \alpha_2, \alpha_3)$ mode occurs at frequencies above the CCMA operating region. The idling interval, α_2, distinguishes this mode from the (α_1, α_3), or CCMA, mode. In DCMA, there is insufficient voltage at the end of the α_1 interval, when D2 opens, to forward bias D1. The output current is zero through the α_2 interval, until sufficient voltage is developed across the magnetizing inductance to forward bias D1, when the α_3 interval commences.

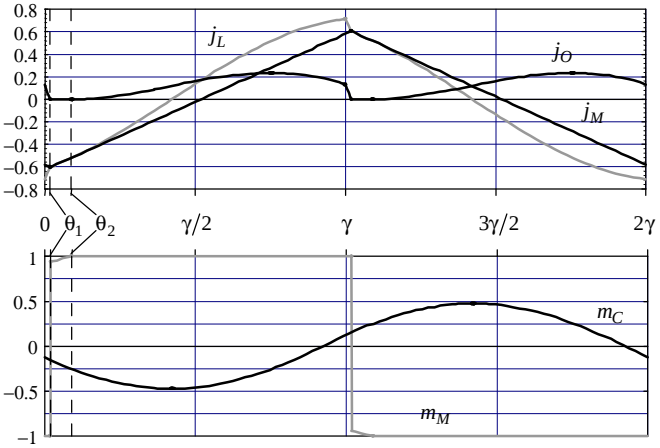

Figure 7: Buck mode DCMA, or $(\alpha_1, \alpha_2, \alpha_3)$ mode, normalized steady-state waveforms $(M = 0.8,\ l = 0.5,\ F = 1.30)$.

At the boundary between CCMA and DCMA, the normalized voltage across the magnetizing inductance at $\theta = \theta_1$ is exactly unity:

$$m_M(\theta_1) = 1 \;\Rightarrow\; \text{CCMA/DCMA boundary} \qquad (27)$$

Using (A.2), this condition can be used to determine the critical value of the dc conversion ratio M_{crit} at which the CCMA/DCMA boundary occurs:

$$M_{\text{crit}} = \frac{1}{\sqrt{1+[2l+l^2+(\gamma l/2)^2]\cos^2(\gamma/2)+(\gamma l/2)\sin\gamma}} \qquad (28)$$

Given values of *M* and *l*, this equation is easily solved numerically for the frequency at which the boundary occurs.

D. Discontinuous Conduction Mode Above and Below Resonance

The DCMAB mode, or $(\alpha_2,\alpha_3,\alpha_4)$ mode occurs above resonance in buck mode, and below resonance in boost mode. In buck mode, the converter transitions from the $(\alpha_1,\alpha_2,\alpha_3)$ to the $(\alpha_2,\alpha_3,\alpha_4)$ when $\alpha_1 \to 0$. By symmetry, if a half-period ends with current flowing in an output diode, it must have begun the cycle with current flowing in the opposite diode. Similarly, if the half-period ends in an idle interval, it must have begun the half-period with either an idle interval, or by going directly into the main power interval. Hence, the α_1 interval (diode current diminishing) will be skipped.

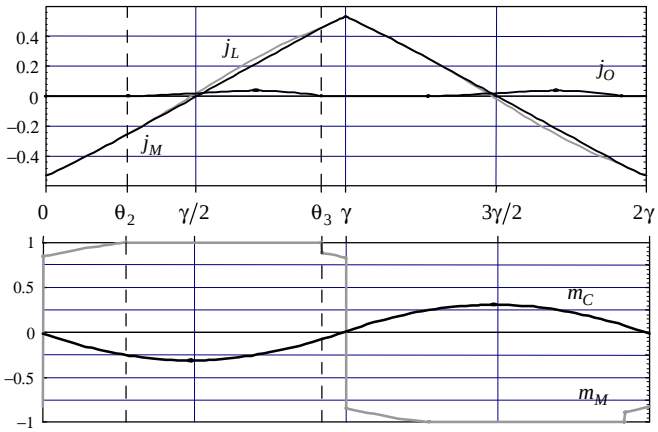

Figure 8: Buck mode DCMAB, or $(\alpha_2,\alpha_3,\alpha_4)$ mode, normalized steady-state waveforms $(M = 0.8, l = 0.5, F = 1.43)$.

E. Cutoff Mode

Cutoff is defined as a mode in which zero power flows to the output. The cutoff frequency is the lowest frequency for which cutoff occurs. Hence, below the cutoff frequency there is power flow to the output, and above it there is none. The cutoff mode consists of a single idle interval, α_2, which persists for the entire half-period. Through an effective inductive voltage divider, the normalized voltage across the magnetizing inductance remains less than unity over the entire half-period, and the output diodes therefore remain open.

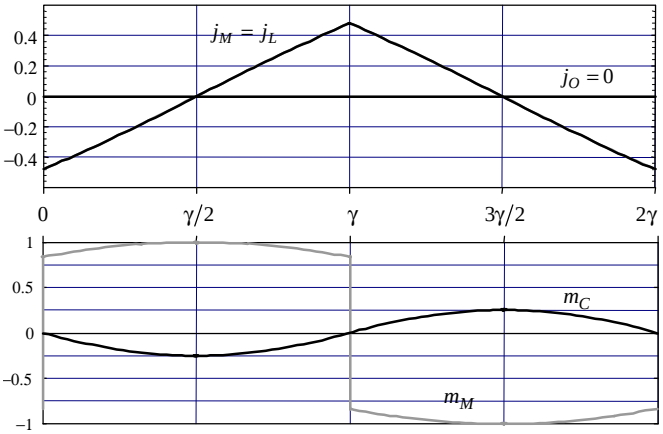

Figure 9: Cutoff mode, or (α_2) mode, normalized steady-state waveforms at the cutoff frequency $(M = 0.8, l = 0.5, F = F_{CO} \cong 1.5484)$.

The solution to the cutoff mode is solvable in closed form. To begin, consider an α_2 interval that spans the entire half-period $0 \le \theta \le \gamma$. The boundary conditions are

$$\begin{aligned} m_C(\gamma) &= -m_C(0) \\ j_L(\gamma) &= -j_L(0) \end{aligned} \qquad (29)$$

Substituting these boundary conditions into the normalized expressions (A.2) for $m_C(\theta)$ and $j_L(\theta)$, and solving for $m_C(0)$ and $j_L(0)$ gives

$$\begin{aligned} m_C(0) &= 0 \\ j_L(0) &= -(k_1/M)\tan(k_1\gamma/2) \end{aligned} \qquad (30)$$

Substituting these values into the expression for $m_M(\theta)$ on the same interval gives the trajectory of the normalized voltage across the magnetizing inductance. It can be shown that the peak value of this trajectory occurs exactly halfway through the half-period, at $\theta = \gamma/2$. At the cutoff frequency, this maximum value is unity, i.e., equal to the normalized output voltage at its peak. That is,

$$m_M(\gamma_{CO}/2) = 1 \qquad (31)$$

Solving for γ_{CO}:

$$\gamma_{CO} = (2/k_1)\cos^{-1}\left(1/(M(1+l))\right) \qquad (32)$$

The cutoff frequency is therefore

$$F_{CO} = \frac{k_1\pi/2}{\cos^{-1}\left(1/(M(1+l))\right)} \qquad (33)$$

Existence of the inverse cosine function requires the magnitude of its argument to be less than unity. A necessary condition for the existence of the cutoff frequency is therefore $M(1+l) > 1$. If this condition is violated, the converter cannot regulate down to zero load, much like the case in the basic two-element SRC.

E. Normalized Output Power

In general, we have the normalized output power

$$p \equiv \frac{P_O}{P_{\text{BASE}}} = \frac{\overline{V_2 i_O}}{V_2^2/R_0} = \frac{\overline{i_O}}{V_2/R_0} = \frac{\overline{i_O}}{I_{\text{BASE}}} = \overline{j_O} \qquad (34)$$

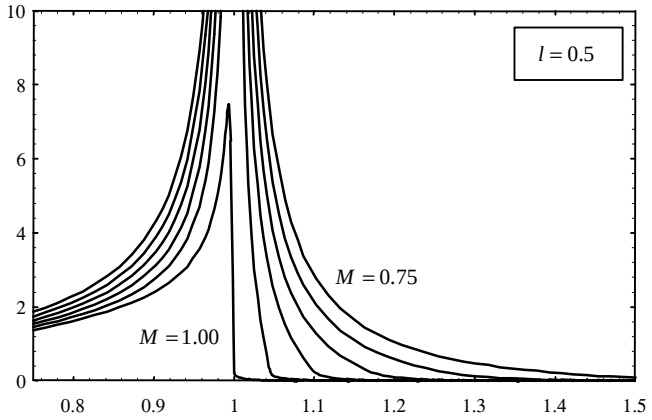

Figure 10: Normalized output power vs. normalized frequency for various values of M in buck mode. ($l = 0.5, M = 1.00, 0.95, 0.90, 0.85, 0.80, 0.75$) .

i.e., the normalized output power is equal to the normalized output current averaged over a half-period

$$p = \overline{j_O} = \frac{1}{\gamma}\int_0^{\gamma} j_O(\theta)\,d\theta \qquad (35)$$

Since no power is delivered during the α_2 and α_4 idling intervals, the normalized output power can be evaluated using

$$p = \frac{1}{\gamma}\int_{\alpha_1} j_O(\theta)\,d\theta + \frac{1}{\gamma}\int_{\alpha_3} j_O(\theta)\,d\theta + \frac{1}{\gamma}\int_{\alpha_5} j_O(\theta)\,d\theta \qquad (36)$$

We can utilize the closed-form results of this section to show that in CCM, the normalized power is given by

$$p = -2m_C(\theta_1)/\gamma \text{ (CCMA)},\ p = 2m_C(\theta_3)/\gamma \text{ (CCMB)} \qquad (37)$$

Figure 10 shows a plot of normalized output power vs. normalized frequency in buck mode. The plot was generated by first finding the steady-state solution through computer iterations, and then applying (36). For values of *M* less than unity, the normalized output power is infinite at the resonant frequency, because the undamped series resonant tank cannot support a driving voltage component at resonance.

V. Boost Mode ($M > 1$)

Within boost mode, there are five different operating modes that commence as the switching frequency is varied from below resonance to cutoff (fig. 11). There is one continuous conduction mode, three discontinuous conduction modes, and the cutoff mode. Three of these modes are the same as those in buck mode, and two are unique to the boost mode.

A. Continuous Conduction Mode Below Resonance

The CCMB, or (α_3, α_5) mode exists within both buck and boost modes, and the analytical results from section IV apply here as well.

B. Discontinuous Conduction Mode Below Resonance 1

The DCMB1, or $(\alpha_3, \alpha_4, \alpha_5)$ mode (fig. 12) is unique to the boost mode of operation. This mode is distinguished from the CCMB (α_3, α_5) mode by the existence of the idle interval α_4. The boundary between these modes can be found using (A.4), and realizing that at the boundary, the normalized voltage across the magnetizing inductance at $\theta = \theta_3$ is exactly -1:

$$m_M(\theta_3) = -1 \ \Rightarrow\ \text{CCMB/DCMB1 boundary} \qquad (38)$$

This leads to exactly the same result (28) found for the buck mode CCMA/DCMA boundary.

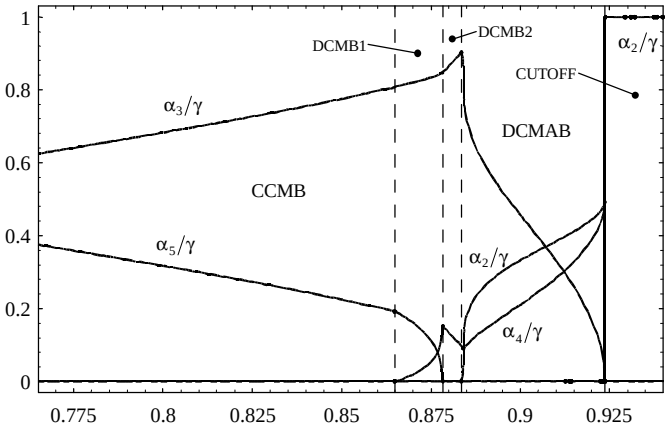

Figure 11: Plot of the normalized conduction intervals α_k/γ vs. normalized frequency F, in boost mode ($M = 1.2,\ l = 0.5$) .

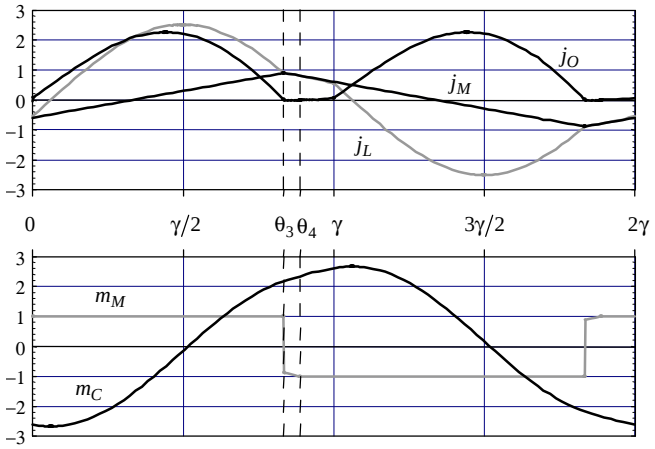

Figure 12: Boost mode DCMB1, or $(\alpha_3, \alpha_4, \alpha_5)$ mode, normalized steady-state waveforms ($M = 1.2, l = 0.5, F = 0.875$) .

C. Discontinuous Conduction Mode Below Resonance 2

The DCMB2, or (α_3, α_4) mode (fig. 13) exists at frequencies above the DCMB1 $(\alpha_3, \alpha_4, \alpha_5)$ mode, and is distinguished by the absence of the α_5 interval. This mode is also unique to the boost mode of operation. Although comprised of only two intervals, analysis of this mode is complicated by a mixture of linear and trigonometric terms. Note that it is not like the CCM case where the magnetizing current is a simple triangle wave. Hence, a closed-form solution was not found.

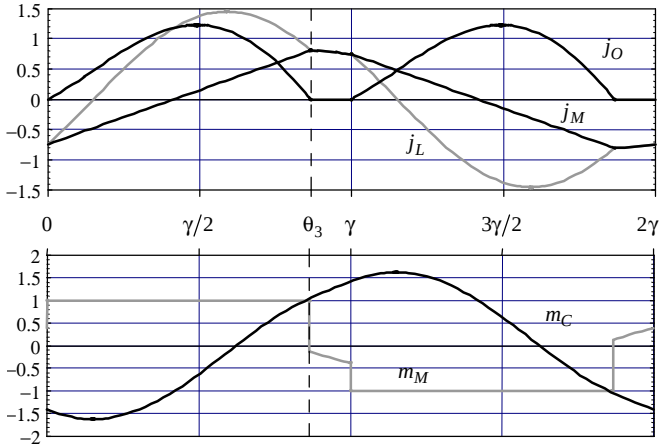

Figure 13: Boost mode DCMB2, or (α_3, α_4) mode, normalized steady-state waveforms $(M = 1.2, l = 0.5, F = 0.88)$.

D. Discontinuous Conduction Mode Above and Below Resonance

As mentioned in section IV, the DCMAB, or $(\alpha_2, \alpha_3, \alpha_4)$ mode occurs above resonance in buck mode, and below resonance in boost mode. This is the light power mode that precedes cutoff. Waveforms in boost mode are similar to those in figure 8 for the buck mode.

E. Cutoff mode

Analysis of the cutoff mode is no different in boost mode than in buck mode, and the results of section IV apply here as well. In figure 11, notice that in boost mode, cutoff can occur below resonance, and zero power is delivered to the output when driven at the resonant frequency of the series tank.

F. Normalized Output Power

A plot of the normalized output power vs. normalized frequency in boost mode is given in figure 14, for various *M*. The plot was generated by iteratively evaluating the equations in the appendix to find the steady-state solution, and then evaluating (36).

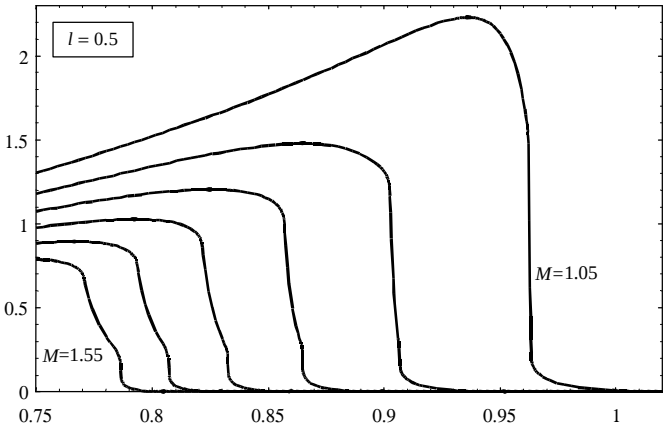

Figure 14: Normalized output power vs. normalized switching frequency for various M in boost mode. $(l = 0.5, M = 1.05, 1.15, 1.25, 1.35, 1.45, 1.55)$.

VI. The $M = 1$ Mode

The $M = 1$ mode obviously marks the boundary between the buck and boost modes. For the case $M = 1$, there are only three operating modes: (a) CCMB, or the (α_3, α_5) mode, (b) DCMAB, or the $(\alpha_2, \alpha_3, \alpha_4)$ mode, and (c) cutoff. Hence, neither modes unique to the boost regime, nor modes unique to the buck regime appear. The transition between CCMB and DCMAB occurs precisely at resonance, and the transition from DCMAB to cutoff occurs at the same cutoff frequency derived in section IV for the buck mode.

VII. Experiment

An experimental half-bridge prototype converter has been designed and tested. It is designed to deliver 600W at 48Vdc from a pre-regulated 400Vdc input. However, as part of an off-line power system, the converter is required to deliver full power over a 275-400Vdc input range, in order to provide hold-up time in the event of a line dropout.

In the design, it is desirable to make the turns-ratio of the transformer large in order to keep the reflected load current on the primary small. With the larger turns-ratio, however, the converter must operate further towards boost mode, where the output power of the converter becomes limited. This is seen in the normalized power curves in figure 14. The converter is designed to operate on the part of the curve where an increase in frequency results in a decrease in output power; i.e., where the derivative of the power curve is negative. This condition must be met at the low-line condition, where the dc conversion ratio is greatest.

A transformer turns-ratio $n = 4$ was chosen for the prototype converter. The component values chosen were: $L = 20\mu\text{H}$, $L_M = 45\mu\text{H}$, and $C = 40\text{nF}$. With the nominal 400Vdc input, the converter operates very close to $M = 1$, and operates into the boost mode when the input voltage is reduced. The measured efficiency of the converter (fig. 15) is highest under the high-line condition. This unusual property is especially useful in applications where the converter spends most of its operating life under this condition.

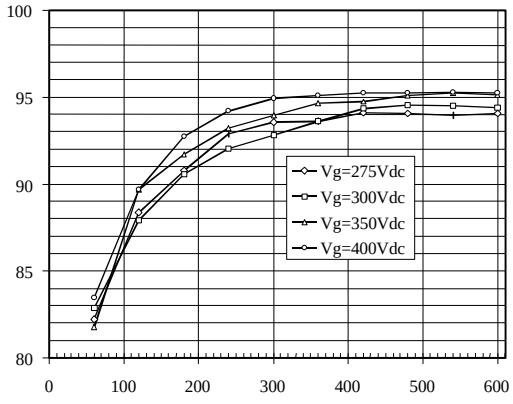

Figure 15: Measured efficiency [%] vs. output power [W] under various line conditions. Note that the highest efficiency is achieved at high-line, 400Vdc.

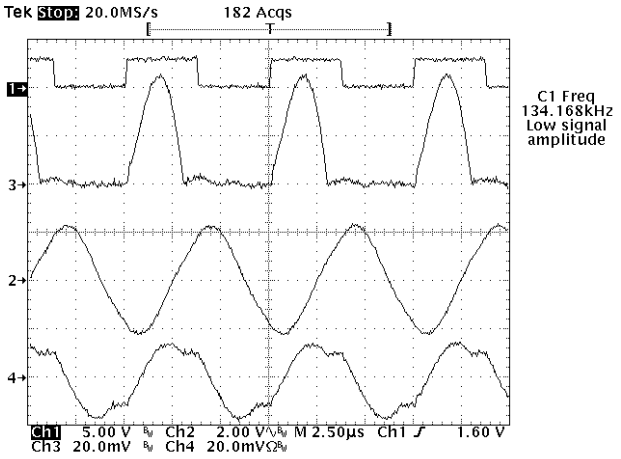

Figure 16: Measured waveforms at full-load and 300Vdc input, in a boost DCMB2 mode: Ch1: Q2 drain-to-source voltage at 500V/div., Ch2: resonant capacitor voltage at 200V/div., Ch3: diode D1 current at 10A/div., Ch4: resonant inductor current at 10A/div.

VIII. Conclusion

An analysis of the steady-state operation of the LLC-SRC has been presented. The analysis was performed in normalized form, which led to the realization that two distinct modes of operation exist, namely the buck mode and the boost mode. The buck and boost modes break down further into the various continuous and discontinuous operating modes, and boundaries between modes were derived analytically, where closed-form solutions were available. Experimental results confirm that this topology can provide a low-cost, high efficiency solution for dc/dc applications.

References

[1] Kurt Schenk, "Investigation of a series loaded half-bridge resonant converter operating above resonance," internal presentation, Caltech Power Electronics Group, December 1997.

[2] Steven D. Johnson and Robert W. Erickson, "Steady-state analysis and design of the parallel resonant converter," IEEE Transactions on Power Electronics, vol.3, No. 1, January 1988, pp. 93-104.

[3] Robert L. Steigerwald, "A comparison of half-bridge resonant converter topologies," IEEE Transactions on Power Electronics, vol.3, No. 2, April 1988, pp. 174-182.

[4] Rudolf P. Severns, "Topologies for three-element resonant converters," IEEE Transactions on Power Electronics, vol.7, No. 1, January 1992, pp. 89-98.

[5] E.G. Schmidtner, "A new high frequency resonant converter topology," HFPC Conference Record, 1988, pp. 9-16.

[6] A.K.S. Bhat, "Analysis and design of LCL-type series resonant converter," IEEE Transactions on Industrial Electronics, vol. 41, No. 1, February 1994, pp. 118-124.

[7] R. Furukoshi, M. Hoshino, P. Greenland, "An application-specific hybrid for the current resonant (smz) converter," Proceedings of 1998 Symposium on Power Semiconductor Devices & IC's, Kyoto, pp. 403-407.

[8] K. Morita, "Novel ultra low-noise soft switch-mode power supply," IEEE Telecommunications Energy Conference, INTELEC 1999, pp. 115-122.

[9] H.-J. Jiang, G. Maggetto, P. Lataire, "Steady-state analysis of the series resonant dc-dc converter in conjunction with loosely coupled transformer-above resonance operation," IEEE Transactions on Power Electronics, vol. 14, No. 3, May 1999, pp. 469-480.

Appendix

The normalized equations describing the converter states in the five intervals that may occur in a half-period are:

$$\left.\begin{aligned} m_C(\theta) &= (m_C(0)-1/M-1)\cos\theta + \\ &\quad j_L(0)\sin\theta + 1/M + 1 \\ m_M(\theta) &= -1 \\ j_L(\theta) &= (-m_C(0)+1/M+1)\sin\theta + j_L(0)\cos\theta \\ j_M(\theta) &= j_M(0) - l\theta \\ j_O(\theta) &= j_M(\theta) - j_L(\theta) \end{aligned}\right\} \quad 0 \le \theta \le \theta_1 \qquad (A.1)$$

$$\left.\begin{aligned} m_C(\theta) &= (m_C(\theta_1)-1/M)\cos k_1(\theta-\theta_1) + \\ &\quad j_L(\theta_1)/k_1 \sin k_1(\theta-\theta_1) + 1/M \\ m_M(\theta) &= \big((1/M - m_C(\theta_1))\cos k_1(\theta-\theta_1) - \\ &\quad j_L(\theta_1)/k_1 \sin k_1(\theta-\theta_1)\big)/(1+l) \\ j_L(\theta) &= (1/M - m_C(\theta_1))k_1 \sin k_1(\theta-\theta_1) + \\ &\quad j_L(\theta_1)\cos k_1(\theta-\theta_1) \\ j_M(\theta) &= j_L(\theta) \\ j_O(\theta) &= 0 \end{aligned}\right\} \quad \theta_1 \le \theta \le \theta_2 \qquad (A.2)$$

$$\left.\begin{aligned} m_C(\theta) &= (m_C(\theta_2)-1/M+1)\cos(\theta-\theta_2) + \\ &\quad j_L(\theta_2)\sin(\theta-\theta_2) + 1/M - 1 \\ m_M(\theta) &= 1 \\ j_L(\theta) &= (1/M - 1 - m_C(\theta_2))\sin(\theta-\theta_2) + \\ &\quad j_L(\theta_2)\cos(\theta-\theta_2) \\ j_M(\theta) &= j_M(\theta_2) + l(\theta-\theta_2) \\ j_O(\theta) &= j_L(\theta) - j_M(\theta) \end{aligned}\right\} \quad \theta_2 \le \theta \le \theta_3 \qquad (A.3)$$

$$\left.\begin{aligned} m_C(\theta) &= (m_C(\theta_3)-1/M)\cos k_1(\theta-\theta_3) + \\ &\quad j_L(\theta_3)/k_1 \sin k_1(\theta-\theta_3) + 1/M \\ m_M(\theta) &= \big((1/M - m_C(\theta_3))\cos k_1(\theta-\theta_3) - \\ &\quad j_L(\theta_3)/k_1 \sin k_1(\theta-\theta_3)\big)/(1+l) \\ j_L(\theta) &= (1/M - m_C(\theta_3))k_1 \sin k_1(\theta-\theta_3) + \\ &\quad j_L(\theta_3)\cos k_1(\theta-\theta_3) \\ j_M(\theta) &= j_L(\theta) \\ j_O(\theta) &= 0 \end{aligned}\right\} \quad \theta_3 \le \theta \le \theta_4 \qquad (A.4)$$

$$\left.\begin{aligned} m_C(\theta) &= (m_C(\theta_4)-1/M-1)\cos(\theta-\theta_4) + \\ &\quad j_L(\theta_4)\sin(\theta-\theta_4) + 1/M + 1 \\ m_M(\theta) &= -1 \\ j_L(\theta) &= (-m_C(\theta_4)+1/M+1)\sin(\theta-\theta_4) + \\ &\quad j_L(\theta_4)\cos(\theta-\theta_4) \\ j_M(\theta) &= j_M(\theta_4) - l(\theta-\theta_4) \\ j_O(\theta) &= j_M(\theta) - j_L(\theta) \end{aligned}\right\} \quad \theta_4 \le \theta \le \gamma \qquad (A.5)$$